Acta Crystallographica Section F
Structural Biology and Crystallization Communications
ISSN 1744-3091

Cloning, expression, purification, crystallization and preliminary X-ray analysis of the human RuvBL1–RuvBL2 complex

Sabine Gorynia,[a,b]* Pedro M. Matias,[a] Tiago M. Bandeiras,[a] Peter Donner[a,b] and Maria Arménia Carrondo[a]

[a]ITQB – Instituto de Tecnologia Química e Biológica, Universidade Nova de Lisboa, Apartado 127, 2781-901 Oeiras, Portugal, and [b]Bayer Schering Pharma, GDD-LGO-LDB-Protein Supply, Muellerstrasse 170-178, 13342 Berlin, Germany

Correspondence e-mail: sabine.gorynia@gmx.de

Received 10 July 2008
Accepted 8 August 2008

The complex of RuvBL1 and its homologue RuvBL2, two evolutionarily highly conserved eukaryotic proteins belonging to the AAA$^+$ (ATPase associated with diverse cellular activities) family of ATPases, was co-expressed in *Escherichia coli*. For crystallization purposes, the flexible domains II of RuvBL1 and RuvBL2 were truncated. The truncated RuvBL1–RuvBL2 complex was crystallized using the hanging-drop vapour-diffusion method at 293 K. The crystals were hexagonal-shaped plates and belonged to either the orthorhombic space group $C222_1$, with unit-cell parameters $a = 111.4$, $b = 188.0$, $c = 243.4$ Å and six monomers in the asymmetric unit, or the monoclinic space group $P2_1$, with unit-cell parameters $a = 109.2$, $b = 243.4$, $c = 109.3$ Å, $\beta = 118.7^\circ$ and 12 monomers in the asymmetric unit. The crystal structure could be solved by molecular replacement in both possible space groups and the solutions obtained showed that the complex forms a dodecamer.

1. Introduction

RuvBL1 and its homologue RuvBL2 are evolutionarily highly conserved eukaryotic proteins belonging to the AAA$^+$ (ATPase associated with diverse cellular activities; Neuwald *et al.*, 1999) family of ATPases. They play important roles in chromatin remodelling and transcription. RuvBL1 and RuvBL2, consisting of 456 and 463 amino acids, respectively, are mainly localized in the nucleus but are also found in the cytosol (Holzmann *et al.*, 1998; Salzer *et al.*, 1999; Kim *et al.*, 2006; Lim *et al.*, 2000). RuvBL2 exhibits 43% identity and 65% similarity to RuvBL1. These proteins were originally identified by several unrelated approaches and are therefore known under diverse names, such as TIP49/TIP48 (Wood *et al.*, 2000; Makino *et al.*, 1998), Pontin52/Reptin52 (Bauer *et al.*, 1998, 2000), TAP54α/TAP54β (Ikura *et al.*, 2000) and Rvb1/Rvb2 (Jonsson *et al.*, 2001).

RuvBL1 and RuvBL2 share homology to the bacterial DNA-dependent ATPase and helicase RuvB (Yamada *et al.*, 2001; Putnam *et al.*, 2001), which is the motor that drives branch migration of the Holliday junction in the presence of RuvA and RuvC during homologous recombination and recombinational repair of damaged DNA (Tsaneva *et al.*, 1993).

The two RuvBL proteins form a complex and act together in various cellular processes, for example in chromatin remodelling. They were found to be present in diverse chromatin-remodelling complexes which regulate chromatin structure and the access of proteins to DNA. The p400 complex is found in animal cells and is essential for E1A-mediated transformation and apoptosis (Fuchs *et al.*, 2001; Samuelson *et al.*, 2005). It is also involved in DNA repair (Kusch *et al.*, 2004) and displays ATPase and helicase activities. It was shown that these functions are at least in part contributed by RuvBL1 and RuvBL2 (Fuchs *et al.*, 2001). RuvBL1 and RuvBL2 are also components of the yeast SWR1 complex and the corresponding SRCAP complex in animals (Jin, Cai, Yao *et al.*, 2005), which remodel chromatin by catalysing ATP-dependent replacement of H2A–H2B histone dimers in nucleosomes by dimers containing the histone variant Htz1 (referred to as H2AZ in mammalian cells; Mizuguchi *et*

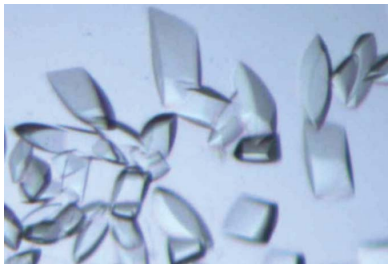

al., 2004; Jin, Cai, Li *et al.*, 2005). In addition, RuvBL1 and RuvBL2 are part of the INO80 complex which exists in yeast and higher eukaryotes. It catalyses the ATP-dependent sliding of nucleosomes along DNA and is involved in the repair of DNA double-strand breaks and in transcriptional regulation (Shen *et al.*, 2000; Jonsson *et al.*, 2001, 2004; Jin, Cai, Yao *et al.*, 2005). It has been shown that RuvBL1 and RuvBL2 are essential for the structural and functional integrity of the INO80 chromatin-remodelling complex (Jonsson *et al.*, 2004). RuvBL1 and RuvBL2 bound to ATP are in the correct conformation to associate with the INO80 complex and initiate the recruitment of the essential actin-like Arp5 subunit to assemble the complete functional chromatin-remodelling complex.

RuvBL1 and RuvBL2 regulate transcription not only *via* association with chromatin-remodelling complexes but also through interactions with diverse transcription factors and the RNA polymerase II holoenzyme complex. RuvBL1 and RuvBL2 were first found to interact with the TATA-binding protein (Kanemaki *et al.*, 1997, 1999) and the large RNA polymerase II holoenzyme complex (Qiu *et al.*, 1998), which contains over 50 components and is responsible for the transcription of protein-encoding genes. Subsequently, RuvBL1 and RuvBL2 were also identified by their physical interaction with the transcription-associated protein β-catenin (Bauer *et al.*, 1998, 2000) and with the transcription factors c-Myc (Wood *et al.*, 2000), E2F1 (RuvBL1 only; Dugan *et al.*, 2002) and ATF2 (RuvBL2 only; Cho *et*

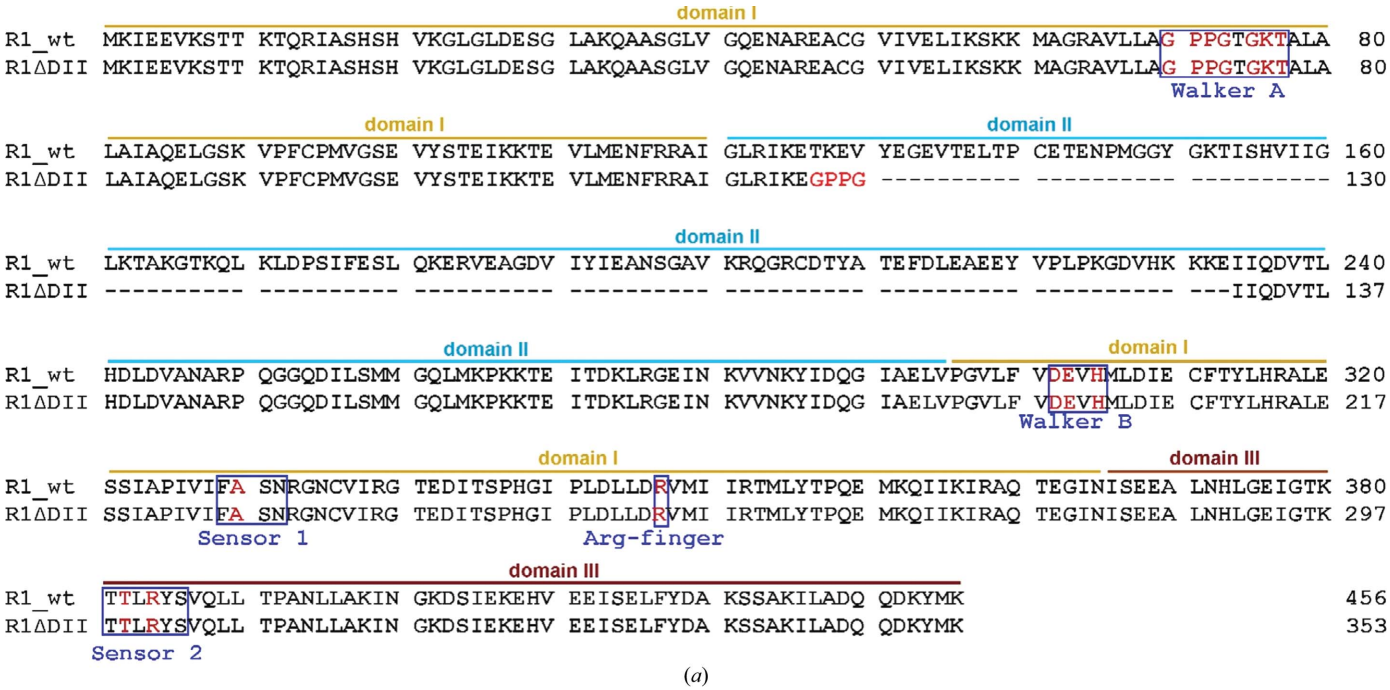

Figure 1
(*a*) Sequence of wild-type RuvBL1 and its ΔDII variant. (*b*) Ribbon diagram of the three-dimensional structure of RuvBL1 (Matias *et al.*, 2006) illustrating its domain structure and arrangement. The domain II region that is truncated to create the ΔDII variant is coloured grey. This figure was prepared with *DINO* (http://www.dino3d.org).

al., 2001). Since then, the mammalian homologues have been implicated in at least two oncogenic pathways, one involving c-Myc and the other involving β-catenin. Among the transcription factors with oncogenic potential, c-Myc is one of the most frequent sites of mutation in human cancer (Cole, 1986).

In this paper, we describe the cloning, expression, purification, crystallization and X-ray analysis of the truncated human RuvBL1–RuvBL2 complex from low-resolution diffraction data.

2. Materials and methods

2.1. Cloning and co-expression of RuvBL1 and RuvBL2

Firstly, the RuvBL1 coding sequence was PCR-amplified using the forward primer 5′-GGCCGGTT**CATATG**AAGATTGAGGAGGTGAAGAGC-3′ and the reverse primer 5′-GCGCGGTT**GGATCC**TTACTTCATGTACTTATCCTGC-3′. The PCR product and the vector pET-15b were cut with the restriction enzymes *Nde*I and *Bam*HI and the RuvBL1 coding region was introduced downstream of the 6×His site in the pET-15b vector (pET15b-6×His-RuvBL1). For co-expression of RuvBL1 and RuvBL2, both genes were cloned into the bicistronic pETDuet vector (Novagen). 6×His-tagged RuvBL1 was PCR-amplified using pET-15b-6×His-RuvBL1 as a template (forward primer 5′-GGGG**CCATGG**TTCATCACCATCACCATC-3′; reverse primer 5′-GGGG**AAGCTT**TTATCACTTCATGTACTTATCCTGCT-3′), digested with *Nco*I and *Hin*dIII and inserted into pETDuet previously cut with the same enzymes. FLAG-tagged RuvBL2 was also PCR-amplified using pET-15b-6×His-FLAG-RuvBL2 as a template (forward primer 5′-GGGG**CATATG**GATTACAAAGACGATGACGATAAAGAAAACCTGTATTTTCAGGGCGCAACCGTTACAGCCACAACC-3′; reverse primer 5′-GGGG**GGTACC**TTATCAGGAGGTGTCCATGGTCTC-3′). Following digestion with *Nde*I and *Kpn*I, RuvBL2 was inserted into the *Nde*I and *Kpn*I restriction sites of pETDuet already containing RuvBL1 (the resulting plasmid was pETDuet-6×His-RuvBL1_FLAG-RuvBL2). For crystallization purposes and functional studies, domain II of both RuvBL1 and RuvBL2 was truncated using overlap extension PCR. The overlap extension PCR consisted of two steps. The forward and reverse primers that annealed to the regions next to the domain II to be excised contained 12 additional nucleotides that were complementary to each other and encoded the amino acids GPPG (highlighted in Fig. 1). For truncation of RuvBL1, the regions next to domain II were amplified in two separate PCRs using the following pairs of primers: R1ΔDII_NcoI_for, 5′-GGGG**CCATGG**TTCATCACCATCACCATC-3′/R1ΔDII_rev, 5′-CCCGGGTGGGCCCTCCTTTATTCGCAGCCCAATGGC-3′ and R1ΔDII_for, 5′-GGCCCACCCGGGATCATCCAAGATGTGACCTTGCATG-3′/R1ΔDII_XhoI_rev, 5′-GGGG**CTCGAG**TTATCACTTCATGTACTTATCCTGCT-3′. In order to truncate the domain II of RuvBL2, the following pairs of primers were used in the initial PCRs: R2ΔDII_NdeI_for, 5′-GGGG**CATATG**GCAACCGTTACAGCCACAACC-3′/R2ΔDII_rev, 5′-CCCGGGTGGGCCCTCCTTGATGCGAACGCCGATGG-3′ and R2ΔDII_for, 5′-GGCCCACCCGGGGTTGTGCACACCGTGTCCCTGC-3′/R2ΔDII_BamHI_rev, 5′-GGGG**GGATCC**TTATCAGGAGGTGTCCATGGTCTC-3′. In a second PCR containing both products from the first PCRs, the flanking parts were not only amplified using R1ΔDII_NcoI_for/R1ΔDII_XhoI_rev and R2ΔDII_NdeI_for/R2ΔDII_BamHI_rev, respectively, but also ligated because of the 12 complementary nucleotides. Both domain II truncation constructs, RuvBL1ΔDII (ΔT127-E233) and RuvBL2ΔDII (ΔE134-E237), were first cloned into the pET-15b vector for expression and solubility tests before cloning both constructs into the bicistronic pETDuet vector for co-expression (as described above). The resulting plasmids were sequenced for verification. For co-expression of RuvBL1 and RuvBL2, the pETDuet vector containing both genes was used to transform *Escherichia coli* BL21 (DE3). *E. coli* cells containing the pETDuet-6×His-RuvBL1ΔDII_FLAG-RuvBL2ΔDII construct were grown overnight at 310 K in 10 ml Luria–Bertani broth supplemented with ampicillin (200 µg ml^{-1}). The cells of this preculture were used to inoculate 400 ml main culture (Luria–Bertani broth containing ampicillin), which was grown to an A_{600} of 0.8 at 310 K for about 2 h. Protein expression was induced with 100 µm isopropyl β-D-1-thiogalactopyranoside and cells were grown for 20 h at 301 K. Using the pETDuet co-expression system, both RuvBL proteins assembled in the cell and formed a stable complex that was purified directly from the cell lysate.

2.2. Purification of the human RuvBL1ΔDII–RuvBL2ΔDII complex

The purified wild-type complex of RuvBL1 and RuvBL2 was used for crystallization trials in order to solve its three-dimensional structure. Although thousands of conditions were tested, the wild-type complex never crystallized. For this reason, deletion mutants of RuvBL1 and RuvBL2 with truncations in their flexible domains II (Matias *et al.*, 2006) were generated: RuvBL1ΔDII lacking residues Thr127–Glu233 and RuvBL2ΔDII lacking Glu134–Glu237. A linker consisting of GPPG was inserted in place of the deleted residues. The proteins remained active with the truncated domain II, but we have not tested whether their nucleotide-binding affinity was affected. RuvBL1ΔDII carrying a N-terminal 6×His tag followed by a thrombin cleavage site (MVHHHHHHLLVPRGS) was co-expressed with RuvBL2ΔDII carrying a N-terminal FLAG tag followed by a TEV cleavage site (MDYKDDDDKENLYFQG). A comparison between wild-type and truncated protein is shown in Fig. 1 for RuvBL1. Three purification steps were necessary to obtain a clean and uniform complex of RuvBL1 and RuvBL2. Cells containing the stable RuvBL1ΔDII–RuvBL2ΔDII complex were harvested by centrifugation (SLA-3000 rotor, Sorvall; 11 000 g; 15 min; room temperature). The wet cells were resuspended in lysis buffer (20 m*M* Tris–HCl pH 8.0, 200 m*M* NaCl, 5% glycerol, 4 m*M* $MgCl_2$, 2 m*M* β-mercaptoethanol and protease-inhibitor cocktail without EDTA from Roche) and disrupted twice in a High-Pressure Laboratory Homogeniser (Rannie) at 75 MPa. Lysates were cleared by centrifugation at 100 000*g* for 45 min with a Beckman 45-Ti rotor. The cleared lysates were loaded onto a Ni–NTA Superflow (Qiagen) column equilibrated in buffer *A* (20 m*M* Tris–HCl pH 8.0, 200 m*M* NaCl, 5% glycerol, 4 m*M* $MgCl_2$, 2 m*M* β-mercaptoethanol, 20 m*M* imidazole pH 8.0). The column was washed with buffer *A* and the bound 6×His-tagged RuvBL1 was eluted with a 20–400 m*M* imidazole gradient. Peak fractions of 6×His-RuvBL1–FLAG-RuvBL2 were collected and loaded onto an anti-FLAG affinity column (Sigma) equilibrated in FLAG buffer (20 m*M* Tris–HCl pH 8.0, 200 m*M* NaCl, 5% glycerol, 4 m*M* $MgCl_2$). The protein was eluted using two column volumes of FLAG peptides (Sigma) dissolved in FLAG buffer (200 µg ml^{-1}). To assure that the purified complex was uniform, size-exclusion chromatography was performed as the last purification step. A HiLoad 16/60 Superdex 200 (Amersham Biosciences) column was equilibrated and run in GF buffer (20 m*M* Tris–HCl pH 8.0, 200 m*M* NaCl, 5% glycerol, 4 m*M* $MgCl_2$, 2 m*M* β-mercaptoethanol). The peak was pooled and concentrated to a final concentration of 20 mg ml^{-1} using an Amicon Ultra Centrifugal Filter with a 30 kDa cutoff. All purification steps were carried out at room temperature and monitored by SDS–PAGE analysis (Fig. 2). The tags were not cleaved before crystallization. We verified the

oligomerization status of the purified complex by gel filtration after keeping it at 277 K for several days. The complex still eluted at the position of a dodecamer, demonstrating that the truncated RuvBL1–RuvBL2 complex was very stable.

2.3. Crystallization

Initial crystallization screens were performed on a 96-well plate at 293 K using a Phoenix nanolitre-drop dispensing robot and allowed the identification of three promising hits from the pH Clear II Screen (Qiagen): A9 (1 *M* LiCl, 0.1 *M* MES pH 6, 10% PEG 6000), A10 (1 *M* LiCl, 0.1 *M* HEPES pH 7, 10% PEG 6000) and A11 (1 *M* LiCl, 0.1 *M* Tris pH 8, 10% PEG 6000). All drops contained 1 *M* LiCl and 10% PEG 6000 as common features, but contained buffers with different pH values. The isolelectric points of RuvBL1ΔDII and RuvBL2ΔDII are 7.4 and 5.2, respectively. The initial results were reproduced and optimized on the microlitre scale using hanging-drop vapour diffusion with a drop composition of 2 µl protein solution (20 mg ml^{-1} RuvBL1ΔDII–RuvBL2ΔDII complex in 20 m*M* Tris–HCl pH 8.0, 200 m*M* NaCl, 5% glycerol, 4 m*M* $MgCl_2$, 2 m*M* β-mercaptoethanol) and 2 µl reservoir solution equilibrated against 500 µl precipitant solution in the well (Fig. 3). Prior to crystallization, 5 m*M* ADP was added to the concentrated protein solution in order to stabilize the complex. The ADP was dissolved in a solution consisting of 50 m*M* Tris pH 8 and 10 m*M* $MgCl_2$. Without ADP addition, no crystal growth occurred. The best diffracting crystals were obtained with a reservoir solution consisting of 0.8 *M* LiCl, 10% PEG 6000 and 0.1 *M* Tris pH 7.5. One crystal obtained under these conditions diffracted to 4 Å resolution and was used to measure diffraction data leading to structure determination. The crystal was a fragment of a thin (∼20 µm) hexagonal-shaped plate (Fig. 3).

Optimization of the RuvBL1ΔDII–RuvBL2ΔDII complex crystals is in progress. Many crystals (100+) grown under different conditions and using different cryoprotecting agents have been screened so far, without success in improving the diffraction resolution. In-house, it was also possible to observe diffraction at room temperature to about 4 Å; however, the crystals were radiation-sensitive and were also extremely sensitive to most cryoprotectants that were tried. Various cryoprotecting agents were tested in pursuit of the best cryosolution possible in order to prevent the formation of ice rings and at the same time avoid significant crystal damage. The RuvBL1ΔDII–RuvBL2ΔDII complex crystals cracked easily upon incubation with cryo-reagents. Reagents such as PEG 400, PEG 400 and glycerol mix, 25% MPD, 30% ethylene glycol, 60% ethanol, sucrose, 2 *M* sodium malonate, 1.25 *M* Li_2SO_4 and LV Cryo Oil from MiTeGen were tested. The cryosolutions were also tested using small stepwise additions of the cryo-reagent to the crystal drop or by incubating the crystals in solutions containing increasing concentrations of cryo-reagent. Fine-tuning of the cryoconditions, most likely containing Li_2SO_4 with or without the presence of other cryo-reagents such as PEG 400, and using a stepwise increase of the cryosolution in the crystallization drop will hopefully yield better diffracting crystals.

2.4. Data collection and preliminary crystallographic analysis

Prior to data collection, a fragment of a thin (∼20 µm) hexagonal-shaped plate crystal of the RuvBL1–RuvBL2 complex with truncated domains II (RuvBL1ΔDII–RuvBL2ΔDII) was flash-frozen in a stream of nitrogen gas at 100 K using a cryoprotecting buffer composed of 0.8 *M* LiCl, 10% PEG 6000, 0.1 *M* Tris pH 7.5 and 20% glycerol. In order to allow the crystal to adjust to the glycerol concentration in the cryoprotecting buffer and avoid cracking, it was dipped briefly into drops containing 0.8 *M* LiCl, 10% PEG 6000, 0.1 *M* Tris pH 7.5 and increasing concentrations (5%, 10%, 15% and 20%) of glycerol. Diffraction data were collected at the European Synchrotron Radiation Facility (ESRF) in Grenoble on beamline ID14-2 at a wavelength of 0.933 Å using an ADSC Quantum 4 detector and were processed to 4 Å resolution with *XDS* (Kabsch, 1993). The diffraction pattern could be indexed and integrated in the

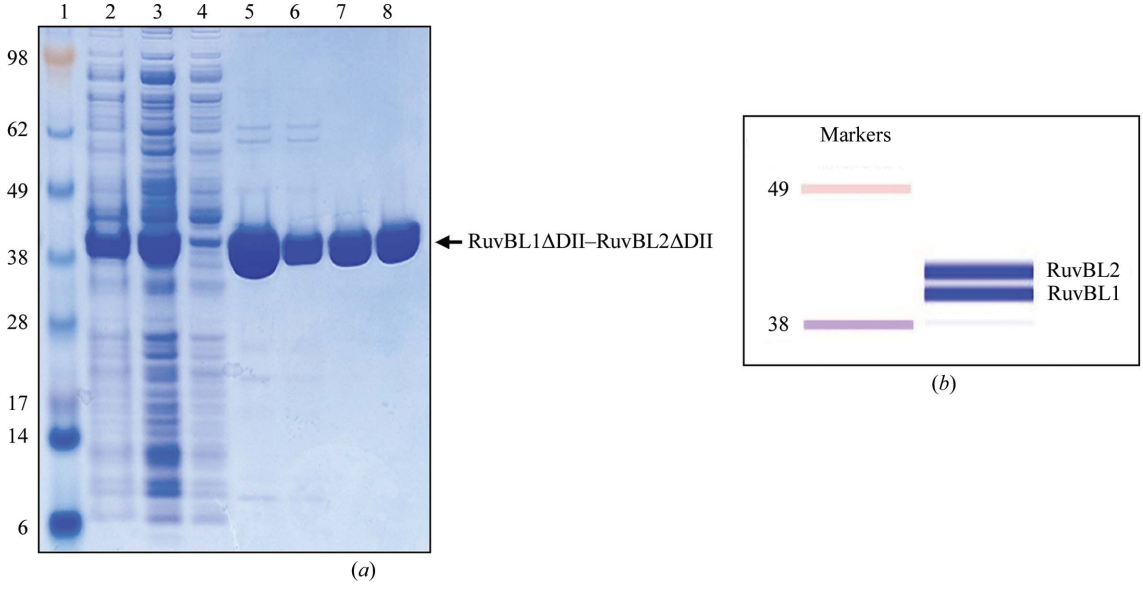

Figure 2
SDS–PAGE of RuvBL1ΔDII–RuvBL2ΔDII complex purification. (*a*) Truncated RuvBL1 and RuvBL2 monomers were not distinguishable in the SDS–PAGE owing to their similar molecular weights of 40.5 and 42.4 kDa, respectively (lane 1 contains molecular-weight markers labelled in kDa). Following cell disruption (lane 2, total sample), the soluble proteins (lane 3) were loaded onto a Ni–NTA column (lane 4, Ni–NTA flowthrough). In the second purification step (anti-FLAG affinity column), all impurities in the Ni–NTA pool (lane 5) and R1ΔDII monomers not associated with the complex were found in the flowthrough (lane 6). To remove the FLAG peptides from the pool of the FLAG column (lane 7, pool FLAG), a gel filtration constituted the last purification step (lane 8, pool GF). (*b*) Automated electrophoresis system capable of separating the RuvBL1 and RuvBL2 bands.

Table 1
Data-collection statistics for the RuvBL1ΔDII–RuvBL2ΔDII complex.

Values in parentheses are for the highest resolution shell.

Beamline and detector	ESRF ID14-2, ADSC Quantum 4	
Wavelength (Å)	0.933	
Resolution (Å)	47.6–3.97 (4.19–3.97)	
Space group	$P2_1$	$C222_1$
Unit-cell parameters		
a (Å)	109.2	111.4
b (Å)	243.4	188.0
c (Å)	109.3	243.4
β (°)	118.7	—
$R_{\rm merge}$†	0.122 (0.360)	0.142 (0.412)
$I/\sigma(I)$	3.5 (2.1)	3.7 (1.8)
No. of observations	88408	88211
No. of unique reflections	38654	21712
Completeness (%)	91.6 (92.3)	99.0 (98.3)
Redundancy	2.3 (2.2)	4.1 (4.1)
$R_{\rm p.i.m.}$†	0.095 (0.279)	0.078 (0.225)
Estimated $B_{\rm overall}$ (Å^2)	84.8	83.5
$V_{\rm M}$ (Å^3 Da^{-1})	2.52	2.52
Solvent content (%)	51.3	51.1

† $R_{\rm merge} = \sum_{hkl}\sum_i |I_i(hkl) - \langle I(hkl)\rangle| / \sum_{hkl}\sum_i I_i(hkl)$, $R_{\rm p.i.m.} = \sum_{hkl}[1/(N-1)]^{1/2} \sum_i |I_i(hkl) - \langle I(hkl)\rangle| / \sum_{hkl}\sum_i I_i(hkl)$, where $I_i(hkl)$ is the observed intensity, $\langle I(hkl)\rangle$ is the average intensity of multiple observations from symmetry-related reflections and N is their redundancy.

orthorhombic space group $C222_1$, with unit-cell parameters a = 111.4, b = 188.0, c = 243.4 Å and six monomers in the asymmetric unit, as well as in the related monoclinic space group $P2_1$, with unit-cell parameters a = 109.2, b = 243.4, c = 109.3 Å, β = 118.7° and 12 monomers in the asymmetric unit. Final data scaling, merging and intensity conversion to structure-factor amplitudes were carried out with *SCALA* and *TRUNCATE* from the *CCP*4 suite (Collaborative Computational Project, Number 4, 1994). A summary of the data-collection and processing statistics is given in Table 1.

2.5. Structure determination

The three-dimensional structure of the RuvBL1ΔDII–RuvBL2ΔDII complex was solved in both possible space groups by the molecular-replacement method using the program *Phaser* (Storoni *et al.*, 2004). The search model was the homologous RuvBL1 monomer (Matias *et al.*, 2006), which was truncated to reflect the shortened domain II region. RuvBL1 has 65% sequence similarity to RuvBL2 and their protein chain lengths are also similar (456 and 463 residues, respectively). Possibly owing to data quality, the molecular-replacement procedure yielded an incomplete solution in both cases, with ten of the expected 12 monomers being located in space group $P2_1$ and five of the expected six monomers in space group $C222_1$ (Table 2). However, inspection of the MR partial solutions on a three-dimensional graphics workstation with *Coot* (Emsley & Cowtan, 2004) showed that the missing monomers could be accommodated in the crystal structure for both space groups without significant clashing or distortion. In order to complete the models, the missing monomers were obtained from three-dimensional superpositions of a truncated RuvBL1 hexamer. The completed models were then input to *Phaser* for refinement and phasing and a marked increase in log-likelihood gain was observed, which is an indication of the correctness of the complete model. In addition, the calculated figure-of-merit statistics obtained with *Phaser* increased from 0.60 to 0.67 in space group $C222_1$ and remained constant at about 0.68 in space group $P2_1$.

3. Results and discussion

Previous structural work using electron-microscopic methods has been carried out on the human RuvBL1–RuvBL2 complex by Puri *et al.* (2007) and similar work has also been reported on the homologous yeast Rvb1–Rvb2 complex by Gribun *et al.* (2008). The structure proposed by Puri and coworkers was dodecameric, with two hexameric rings facing each other. Furthermore, the results reported by these authors indicated that the dodecamers were asymmetrical (*i.e.* the two hexameric rings were not identical in shape), which would seem to favour the possibility of two homohexameric rings, one made up of RuvBL1 monomers and the other made up of RuvBL2 monomers. On the other hand, Gribun and coworkers proposed that the Rvb1–Rvb2 complex was a heterohexamer, probably made up of alternating RuvBL1 and RuvBL2 monomers.

In our RuvBL1ΔDII–RuvBL2ΔDII complex crystal structure a dodecamer was clearly identified. However, the expected high similarity between the three-dimensional structures of the DII-truncated

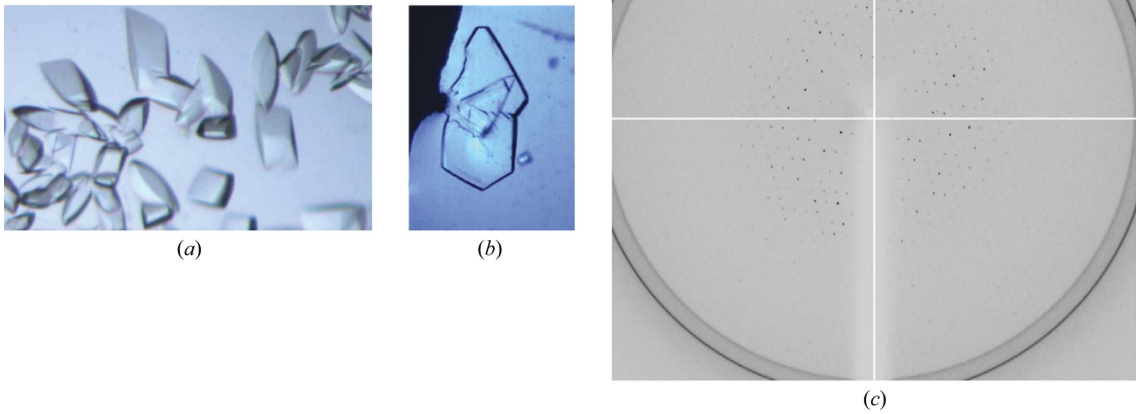

(*a*) (*b*) (*c*)

Figure 3
Crystals and diffraction pattern of the RuvBL1ΔDII–RuvBL2ΔDII complex. (*a*) RuvBL1ΔDII–RuvBL2ΔDII crystals. (*b*) Optimized RuvBL1ΔDII–RuvBL2ΔDII hexagonal-shaped plates used for structure determination. (*c*) The crystal diffracted to 4 Å resolution. The ice rings surrounding the diffraction pattern may be the consequence of accidental thawing and freezing of the crystal in the loop and may prevent the observation of spots at a slightly higher resolution of about 3.5 Å.

forms of RuvBL1 and RuvBL2 combined with the data quality and resolution made the distinction between RuvBL1 and RuvBL2 monomers as well as between space groups $C222_1$ and $P2_1$ rather difficult. The complex may crystallize in space group $C222_1$ or in $P2_1$ with $C222_1$ pseudo-symmetry. In addition, the actual space group will have significant implications in the complex structure. The main noncrystallographic symmetry axis of the dodecamer is not parallel to the long cell edge (b = 243.4 Å in $P2_1$, c = 243.4 Å in $C222_1$), although it does make a small (∼16°) angle with it. In $P2_1$, with 12 monomers (six RuvBL1ΔDII and six RuvBL2ΔDII) in the asymmetric unit, there are three possibilities: either a dodecamer with sixfold noncrystallographic symmetry made of one homohexameric ring of RuvBL1ΔDII monomers facing a homohexameric ring of RuvBL2ΔDII monomers or a dodecamer with 32 noncrystallographic symmetry formed by two crystallographically independent heterohexameric rings facing each other and composed of alternating RuvBL1ΔDII and RuvBL2ΔDII monomers in two possible different arrangements. However, in $C222_1$, with six monomers (three RuvBL1ΔDII and three RuvBL2ΔDII) in the asymmetric unit, the only possibility is that of a heterohexameric ring composed of alternating RuvBL1ΔDII and RuvBL2ΔDII monomers facing a heterohexamer related by a crystallographic twofold axis to complete a dodecamer with 32 noncrystallographic symmetry.

Self-rotation calculations with both *MOLREP* (Fig. 4) and *POLARRFN* (not shown) from *CCP*4 appear to support the double-heterohexamer hypothesis in $C222_1$: the peaks in the κ = 60, 120 and 180° sections are much stronger than in $P2_1$ and the *MOLREP* maps are more detailed, especially in $C222_1$ when integration radii greater than 40 Å are used, where it can be seen that the peaks in the κ = 120° section are stronger than those in the κ = 60° and also that the peaks are offset from the crystallographic twofold axis c and thus not parallel to it. In addition, no strong peaks in the native Patterson function are observed in either space group.

Table 2
Molecular-replacement results.

Phaser log-likelihood function (LLG) *versus* the number of correctly placed monomers in the model.

Monomers in MR solution	LLG in $P2_1$	LLG in $C222_1$
1	50.17	90.89
2	153.98	270.17
3	303.99	504.28
4	466.68	793.12
5	688.06	1089.98
6	923.51	1602.08†
7	1172.87	
8	1429.58	
9	1713.69	
10	1807.39‡	
11	nd	
12	2716.31†	

† After refinement and phasing with completed model (see text for details). ‡ After refinement and phasing with the ten best monomers.

The modified RuvBL1 hexamer (see §2.5 above) was also tried as a MR search model in both $P2_1$ (two copies) and $C222_1$ (one copy). Both calculations gave a solution, but it was decided to use the monomer in the hope that the order in which the solutions were found would hint at the dodecamer composition, the rationale being

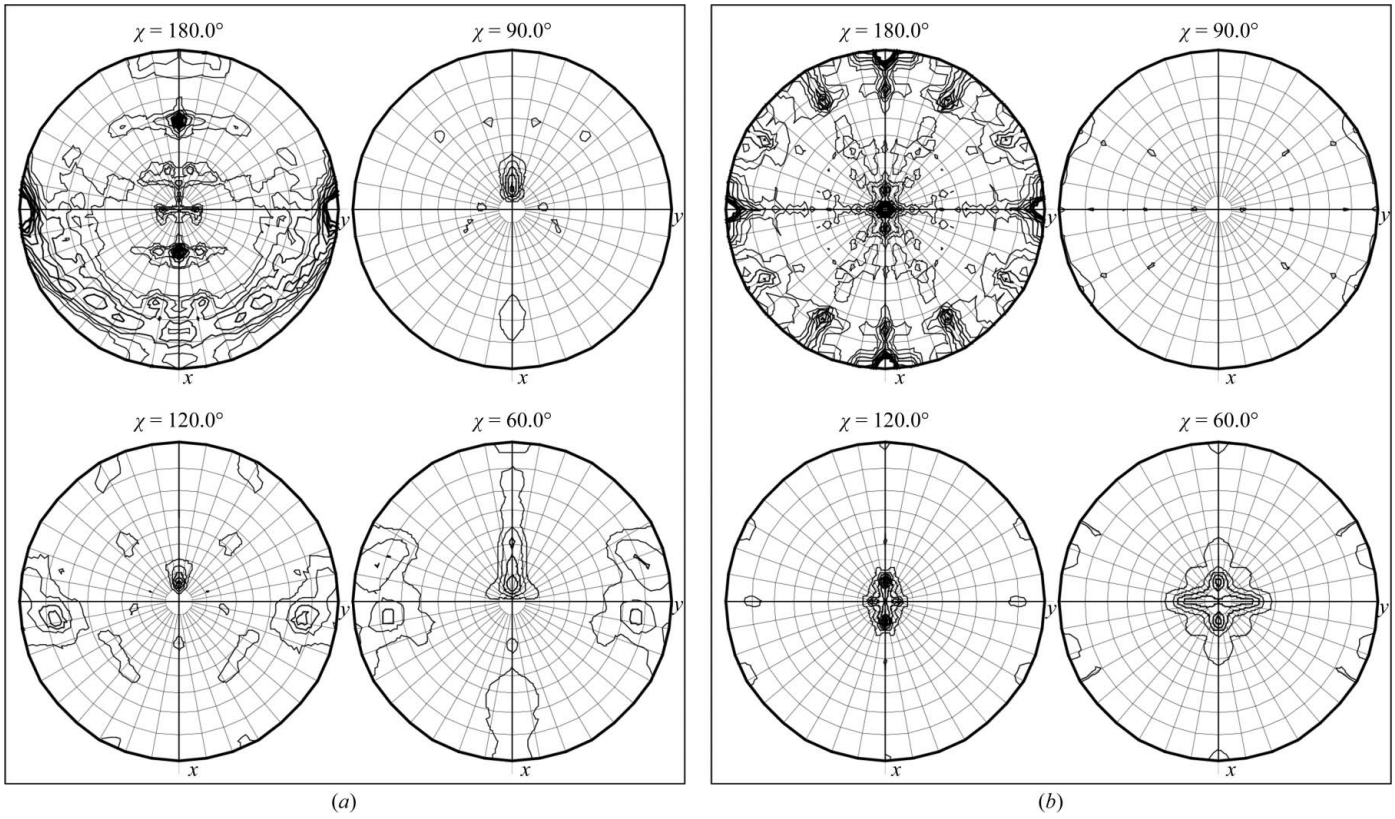

Figure 4
Self-rotation function calculations with *MOLREP*. (*a*) Space group $P2_1$; (*b*) space group $C222_1$. The contour levels are drawn at unit intervals between 1 and 6 map r.m.s. Owing to the different coordinate axial conventions, the plots are not directly comparable. In $P2_1$, the crystallographic twofold along unit-cell direction b can be seen as strong peaks at the sides of the κ = 180° section in (*b*). This axis corresponds to the crystallographic c axis in $C222_1$, which is at the centre of the κ = 180° section in (*a*). The strong peaks along the vertical axis on the $P2_1$ κ = 180° section represent noncrystallographic twofold axes in $P2_1$ which become crystallographic in $C222_1$ along unit-cell directions a and b.

that the RuvBL1 monomers might be located first. However, the interpretation of these results was inconclusive. Finally, the low resolution of the data discouraged the use of model building and refinement as a means of resolving these ambiguities; therefore, crystal optimization aimed at data collection to higher resolution is currently under way. Since we could not identify the RuvBL1ΔDII and RuvBL2ΔDII monomers and carry out model rebuilding and refinement, no coordinates have been submitted to the Protein Data Bank at this stage.

This work was supported by European Commission funding through the SPINE2-COMPLEXES project LSHG-CT-2006-031220.

References

Bauer, A., Chauvet, S., Huber, O., Usseglio, F., Rothbacher, U., Aragnol, D., Kemler, R. & Pradel, J. (2000). *EMBO J.* **19**, 6121–6130.

Bauer, A., Huber, O. & Kemler, R. (1998). *Proc. Natl Acad. Sci. USA*, **95**, 14787–14792.

Cho, S. G., Bhoumik, A., Broday, L., Ivanov, V., Rosenstein, B. & Ronai, Z. (2001). *Mol. Cell. Biol.* **21**, 8398–8413.

Cole, M. D. (1986). *Annu. Rev. Genet.* **20**, 361–384.

Collaborative Computational Project, Number 4 (1994). *Acta Cryst.* D**50**, 760–763.

Dugan, K. A., Wood, M. A. & Cole, M. D. (2002). *Oncogene*, **21**, 5835–5843.

Emsley, P. & Cowtan, K. (2004). *Acta Cryst.* D**60**, 2126–2132.

Fuchs, M., Gerber, J., Drapkin, R., Sif, S., Ikura, T., Ogryzko, V., Lane, W. S., Nakatani, Y. & Livingston, D. M. (2001). *Cell*, **106**, 297–307.

Gribun, A., Cheung, K. L., Huen, J., Ortega, J. & Houry, W. A. (2008). *J. Mol. Biol.* **376**, 1320–1333.

Holzmann, K., Gerner, C., Korosec, T., Poltl, A., Grimm, R. & Sauermann, G. (1998). *Biochem. Biophys. Res. Commun.* **252**, 39–45.

Ikura, T., Ogryzko, V. V., Grigoriev, M., Groisman, R., Wang, J., Horikoshi, M., Scully, R., Qin, J. & Nakatani, Y. (2000). *Cell*, **102**, 463–473.

Jin, J., Cai, Y., Li, B., Conaway, R. C., Workman, J. L., Conaway, J. W. & Kusch, T. (2005). *Trends Biochem. Sci.* **30**, 680–687.

Jin, J., Cai, Y., Yao, T., Gottschalk, A. J., Florens, L., Swanson, S. K., Gutierrez, J. L., Coleman, M. K., Workman, J. L., Mushegian, A., Washburn, M. P., Conaway, R. C. & Conaway, J. W. (2005). *J. Biol. Chem.* **280**, 41207–41212.

Jonsson, Z. O., Dhar, S. K., Narlikar, G. J., Auty, R., Wagle, N., Pellman, D., Pratt, R. E., Kingston, R. & Dutta, A. (2001). *J. Biol. Chem.* **276**, 16279–16288.

Jonsson, Z. O., Jha, S., Wohlschlegel, J. A. & Dutta, A. (2004). *Mol. Cell*, **16**, 465–477.

Kabsch, W. (1993). *J. Appl. Cryst.* **26**, 795–800.

Kanemaki, M., Kurokawa, Y., Matsu-ura, T., Makino, Y., Masani, A., Okazaki, K., Morishita, T. & Tamura, T. A. (1999). *J. Biol. Chem.* **274**, 22437–22444.

Kanemaki, M., Makino, Y., Yoshida, T., Kishimoto, T., Koga, A., Yamamoto, K., Yamamoto, M., Moncollin, V., Egly, J. M., Muramatsu, M. & Tamura, T. (1997). *Biochem. Biophys. Res. Commun.* **235**, 64–68.

Kim, J. H., Choi, H. J., Kim, B., Kim, M. H., Lee, J. M., Kim, I. S., Lee, M. H., Choi, S. J., Kim, K. I., Kim, S. I., Chung, C. H. & Baek, S. H. (2006). *Nature Cell Biol.* **8**, 631–639.

Kusch, T., Florens, L., MacDonald, W. H., Swanson, S. K., Glaser, R. L., Yates, J. R. III, Abmayr, S. M., Washburn, M. P. & Workman, J. L. (2004). *Science*, **306**, 2084–2087.

Lim, C. R., Kimata, Y., Ohdate, H., Kokubo, T., Kikuchi, N., Horigome, T. & Kohno, K. (2000). *J. Biol. Chem.* **275**, 22409–22417.

Makino, Y., Mimori, T., Koike, C., Kanemaki, M., Kurokawa, Y., Inoue, S., Kishimoto, T. & Tamura, T. (1998). *Biochem. Biophys. Res. Commun.* **245**, 819–823.

Matias, P. M., Gorynia, S., Donner, P. & Carrondo, M. A. (2006). *J. Biol. Chem.* **281**, 38918–38929.

Mizuguchi, G., Shen, X., Landry, J., Wu, W. H., Sen, S. & Wu, C. (2004). *Science*, **303**, 343–348.

Neuwald, A. F., Aravind, L., Spouge, J. L. & Koonin, E. V. (1999). *Genome Res.* **9**, 27–43.

Puri, T., Wendler, P., Sigala, B., Saibil, H. & Tsaneva, I. R. (2007). *J. Mol. Biol.* **366**, 179–192.

Putnam, C. D., Clancy, S. B., Tsuruta, H., Gonzalez, S., Wetmur, J. G. & Tainer, J. A. (2001). *J. Mol. Biol.* **311**, 297–310.

Qiu, X. B., Lin, Y. L., Thome, K. C., Pian, P., Schlegel, B. P., Weremowicz, S., Parvin, J. D. & Dutta, A. (1998). *J. Biol. Chem.* **273**, 27786–27793.

Salzer, U., Kubicek, M. & Prohaska, R. (1999). *Biochim. Biophys. Acta*, **1446**, 365–370.

Samuelson, A. V., Narita, M., Chan, H. M., Jin, J., de Stanchina, E., McCurrach, M. E., Fuchs, M., Livingston, D. M. & Lowe, S. W. (2005). *J. Biol. Chem.* **280**, 21915–21923.

Shen, X., Mizuguchi, G., Hamiche, A. & Wu, C. (2000). *Nature (London)*, **406**, 541–544.

Storoni, L. C., McCoy, A. J. & Read, R. J. (2004). *Acta Cryst.* D**60**, 432–438.

Tsaneva, I. R., Muller, B. & West, S. C. (1993). *Proc. Natl Acad. Sci. USA*, **90**, 1315–1319.

Wood, M. A., McMahon, S. B. & Cole, M. D. (2000). *Mol. Cell*, **5**, 321–330.

Yamada, K., Kunishima, N., Mayanagi, K., Ohnishi, T., Nishino, T., Iwasaki, H., Shinagawa, H. & Morikawa, K. (2001). *Proc. Natl Acad. Sci. USA*, **98**, 1442–1447.